ADVANCED THERAPEUTICS
www.advtherap.com

Discovery of Broad-Spectrum Repurposed Drug Combinations Against Carbapenem-Resistant *Enterobacteriaceae* (CRE) Through Artificial Intelligence (AI)-Driven Platform

Ming Li, Kui You, Peter Wang, Lissa Hooi, Yahua Chen, Anqi Siah, Shi-Bei Tan, Jeanette Teo, Oon-Tek Ng, Kalisvar Marimuthu, Indumathi Venkatachalam, Agata Blasiak, Edward Kai-Hua Chow,* Dean Ho,* and Yunn-Hwen Gan**

Antimicrobial resistance challenges the sustainability of healthcare systems and results in substantial economic losses worldwide. This issue is further aggravated by paucity of new drugs and treatment options. In this study, an artificial intelligence (AI)-derived platform termed IDentif.AI is utilized to accelerate the development of effective therapeutic options for carbapenem-resistant *Enterobacteriaceae* (CRE). Twelve Food and Drug Administration-approved drugs are selected and the in vitro inhibitory efficacy of 155 combinations consisting of various drugs is determined at different concentrations against both *Klebsiella pneumoniae* and *Escherichia coli*. Correlating these experimental data via an AI-derived relationship, IDentif.AI rapidly determines a ranked list of drug combinations in the search space of over half a million possible combinations. Meropenem is found to strongly synergize with low doses of the anticancer drug bleomycin, showing broad-spectrum, bactericidal activity against nine isolates across three CRE species in rich and minimal media with no synergistic cytotoxicity on mammalian cells. Synergy is also detected between bleomycin and other key carbapenems in clinical use (imipenem, ertapenem). Bleomycin/carbapenem appears to be a promising combination therapy for treating various CRE infections. IDentif.AI shows profound capability of identifying pan-active drug combinations against a family of bacteria through surveying strains from different species in parallel.

1. Introduction

The extensive spread of resistance to antibiotics across the globe is bringing us closer to the "post-antibiotic" era where common and even minor infections may become deadly.[1] If no effective intervention strategies for AMR are implemented by 2050, we may see the loss of 10 million lives per annum.[2] Of particular concern is the emerging resistance to carbapenems, which are considered the last-resort antibiotics for treating multi drug resistant (MDR) Gram-negative bacterial infections. In 2017, the WHO issued the Global Priority List of Antibiotic Resistant Bacteria, among which CRE has been highlighted as critical priority pathogens demanding an urgent therapeutic response.[3]

CRE infections are primarily acquired in healthcare settings.[4] Poor treatment outcomes and up to 50% mortality rates have been frequently reported, especially in patients who are critically ill.[5–7] Despite the absence of a standardized anti-CRE treatment, reported clinical outcomes have pointed to the enhanced treatment

M. Li, Y. Chen, A. Siah, Y.-H. Gan
Department of Biochemistry
Yong Loo Lin School of Medicine
National University of Singapore
Singapore 117596, Singapore
E-mail: bchganyh@nus.edu.sg

The ORCID identification number(s) for the author(s) of this article can be found under https://doi.org/10.1002/adtp.202300332

DOI: 10.1002/adtp.202300332

M. Li, Y. Chen, A. Siah, Y.-H. Gan
Infectious Diseases Translational Research Programme
Yong Loo Lin School of Medicine
National University of Singapore
Singapore 117549, Singapore

K. You, P. Wang, S.-B. Tan, A. Blasiak, E. K.-H. Chow, D. Ho
The Institute for Digital Medicine (WisDM)
Yong Loo Lin School of Medicine
National University of Singapore
Singapore 117456, Singapore
E-mail: agata.blasiak@nus.edu.sg; edwardkchow@nus.edu.sg; biedh@nus.edu.sg

K. You, P. Wang, S.-B. Tan, A. Blasiak, E. K.-H. Chow, D. Ho
The N.1 Institute for Health (N.1)
National University of Singapore
Singapore 117456, Singapore

effectiveness of combinatorial therapies when compared to monotherapies.[8,9] Furthermore, current combinatorial drug treatment for CRE infections revolves around the following strategies: 1) high-dose carbapenem (such as meropenem) in combination with antibiotics that are active in vitro (such as colistin, tigecycline), 2) double carbapenems (such as meropenem/ertapenem), and 3) β-lactam with β-lactam inhibitor (such as ceftazidime-avibactam).[10] These strategies, however, result in variable clinical outcomes and are confronted with resistance issue.

Typically, developing a new drug consists of several in vitro and in vivo validations and phases of clinical trials, and the timeline requires 10–15 years. However, such a prolonged timeline is insufficient to address the rapid emergence of AMR pathogens. Recently, high-throughput screening and higher-order drug development approaches have contributed to designing effective repurposed drug combinations.[11–14] Optimizing drug combinations, especially for AMR infections with the rapid emergence of mutations and strains, is a challenging task. For instance, designing combinations from a pool of 12 drugs with three dosage levels requires the screening of more than half a million ($3^{12} = 531\,441$) combinations, which is an insurmountable task in the context of drug development. To address this challenge, we harnessed an AI-derived platform, IDentif.AI, to pinpoint and design effective anti-CRE combination therapies. IDentif.AI utilizes a second-order quadratic relationship to correlate input drug combinations and their corresponding biological response (e.g., % Inhibition) to pinpoint effective regimens. This correlation was first discovered via neural network on the relationship between cellular response and input therapeutics, and it has been validated in other in vitro and in vivo studies pertaining to infectious diseases and cancer.[15–30] The second order quadratic relationship was also confirmed via prospective human studies.[31–37] This platform is mechanism agnostic and does not rely on pre-existing data or in silico modeling. All results from IDentif.AI are based on prospectively obtained experimental data, and pinpointed combinations are optimal within the selected pool of drugs.

In this study, 12 FDA-approved drugs were selected and concentrations at 5% and 10% C_{max} or inhibitory concentration IC_{10} and IC_{20} were tested for combinatorial design. The IDentif.AI workflow pinpointed low concentrations of bleomycin (BLM) in combination with meropenem (MEM) as the top effective and synergistic combination across different *Enterobacteriaceae* species and strains. No cytotoxicity or cytotoxic synergy was seen in mammalian cells with the BLM and MEM doses used in the combination. BLM/MEM thus appears to be a promising combinatorial therapy for treating various CRE infections and could be further tested in preclinical models to examine the potential clinical suitability of the combination (e.g., toxicity). This study further demonstrates the potential of using the IDentif.AI platform as an alternative, rapid approach to determine novel drug combinatorial designs for CRE-related infections.

2. Results

2.1. Two Selected CRE Strains, 12 FDA-approved Drugs, and Drug Concentration Selection for IDentif.AI

We selected *K. pneumoniae* (ENT646) and *E. coli* (C31) clinical isolates as representative multi-drug resistant CRE to determine novel and effective drug combinations that may be broadly active against various CRE species (**Figure 1**). Both ENT646 and C31 carry genes resistant to more than three classes of antibiotics (Table S1, Supporting Information). ENT646 is a hypervirulent *K. pneumoniae* (hv*Kp*) isolate,[38] an example of the alarming emergence of "superbugs" due to the increasing convergence of hypervirulence and carbapenem resistance in *K. pneumoniae*.[38–40]

The initial pool of 12 drugs was selected from three groups: 1) mainstay antibiotics essential for treating CRE infections, such as MEM and polymyxin B (PB);[8,9,41] 2) drug sensitizers, such as efflux pump inhibitor metformin;[42] and 3) repurposed drugs reported with antibacterial activity (**Table 1**). IDentif.AI assesses three clinically relevant drug concentrations. Aside from data derived from dose-response curves (Figure S1, Supporting Information), C_{max} values obtained from regulatory documents and clinical trials also served as one of the concentration selection parameters. Typically, 10% of C_{max} is considered the achievable

K. You, P. Wang, S.-B. Tan, A. Blasiak, E. K.-H. Chow, D. Ho
Department of Biomedical Engineering
College of Design and Engineering
National University of Singapore
Singapore 117583, Singapore
L. Hooi
Cancer Science Institute of Singapore
National University of Singapore
Singapore 117599, Singapore
J. Teo
National University Hospital
Singapore 169857, Singapore
O.-T. Ng, K. Marimuthu
National Centre for Infectious Diseases
Singapore 308442, Singapore
K. Marimuthu
Tan Tock Seng Hospital
Singapore 308433, Singapore
K. Marimuthu
Lee Kong Chian School of Medicine
Nanyang Technological University
Singapore 636921, Singapore
I. Venkatachalam
Department of Infectious Diseases
Singapore General Hospital
Singapore 169608, Singapore
A. Blasiak, E. K.-H. Chow, D. Ho
Department of Pharmacology
Yong Loo Lin School of Medicine
National University of Singapore
Singapore 117600, Singapore
E. K.-H. Chow
NUS Centre for Cancer Research (N2CR)
Yong Loo Lin School of Medicine
National University of Singapore
Singapore 117599, Singapore
D. Ho
Bia-Echo Asia Centre for Reproductive Longevity and Equality (ACRLE)
Yong Loo Lin School of Medicine
National University of Singapore
Singapore 117456, Singapore

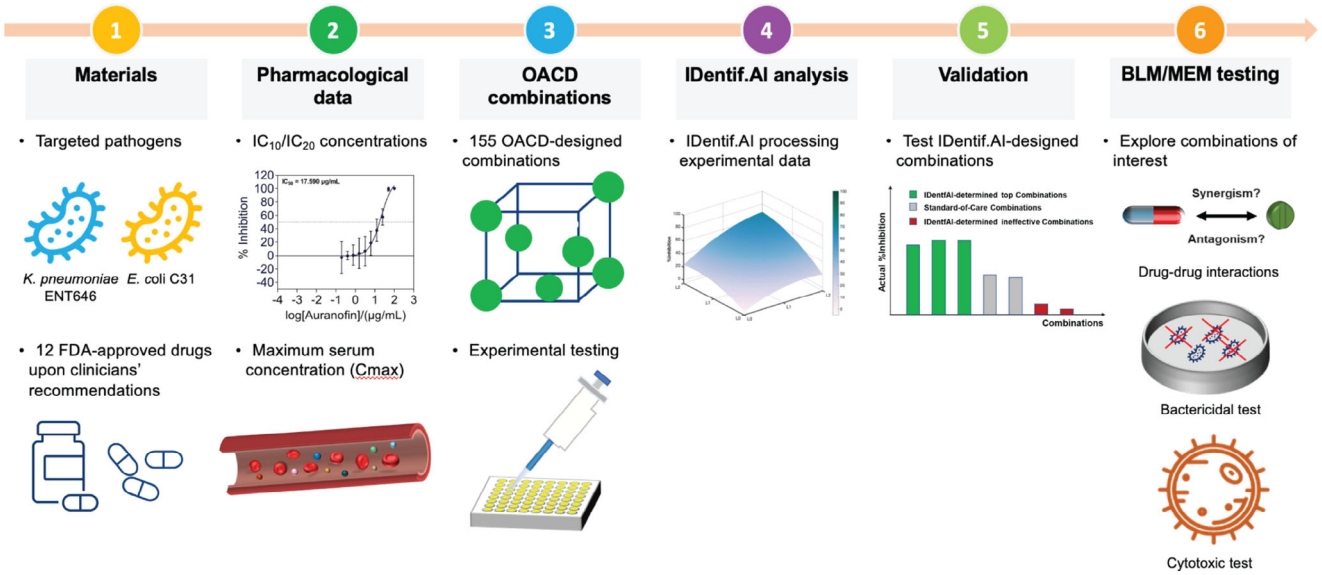

Figure 1. Workflow of the IDentif.AI-guided drug combinatorial study against CRE. Two clinical isolates from the most representative CRE species (hv*Kp* ENT646 and *E. coli* C31) are investigated by IDentif.AI. The workflow begins by selecting 12 FDA-approved drugs, and they are individually assessed via dose-response experiment in vitro. Relevant concentration levels are selected. Subsequently, 155 OACD-designed combinations are experimentally validated, and the respective data are analyzed by IDentif.AI. Top combinations selected by the platform are comprehensively analyzed.

concentration of administered drug in the targeted site.[16,27] The three concentration levels are level 0 (absence of the drug in a combination), level 1, and level 2 concentrations. Level 1 and level 2 concentrations are selected based on the lower of the two values: 5%/10% C_{max} or IC_{10}/IC_{20}. The integration of pharmacological (5%/10% C_{max}) and potency data (IC_{10}/IC_{20}) ensures that identified therapies are clinically actionable and no single agents are over-represented. Notably, inactive drugs that have no antibacterial activity in vitro are also considered by IDentif.AI as drug interactions may occur when drugs are properly paired in combinations and at the correct concentrations.

2.2. Optimization and Experimental Validation of IDentif.AI-pinpointed Combinations

The monotherapies for each of the 12 drugs at level 1 and level 2 concentrations generally demonstrated low efficacy (less than 24% Inhibition) against both ENT646 and C31 isolates ($N = 3$; Figure S2, Supporting Information). However, pairing them in combinations may result in enhanced efficacy. IDentif.AI harnessed the experimental data of the 155 orthogonal array composite design (OACD) combinations consisting of drugs at three concentration levels (Table S2, Supporting Information) against

Table 1. 12 FDA-approved clinical-in-use drugs with their selected level 1 and level 2 concentrations.

Pharmacological data [μg mL^{-1}]				Hv*Kp* ENT646 [μg mL^{-1}]			*E. coli* C31 [μg mL^{-1}]		
Drug	C_{max}	5% C_{max}	10% C_{max}	IC_{10}	IC_{20}	IC_{50}	IC_{10}	IC_{20}	IC_{50}
ARF	0.312[43]	0.0156	0.0312	5.334	9.179[b)]	26.250	4.295	7.291[b)]	17.590
ATS	3.300[44]	0.165	0.330	>100	>100[b)]	>100	13.610	27.020[b)]	74.060
BLM	1000[45]	50	100	0.100	0.183[a)]	0.413	16.370	>100[b)]	>100
CPX	0.221[46]	0.0111	0.0221	5.267	5.697[b)]	6.804	6.406	6.613[b)]	7.079
FUDR	0.259[45]	0.0130	0.0259	0.196	0.286[b)]	0.574	0.197	0.261[b)]	0.360
LVX	9.300[47]	0.465	0.930	0.607	0.768[a)]	1.208	10.060	11.300[b)]	13.900
MTF	1.301[48]	0.0651	0.130	>100	>100[b)]	>100	>100	>100[b)]	>100
MEM	61.6[49]	3.080	6.160	0.227	1.283[a)]	3.799	20.010	26.690[b)]	36.950
PMB	8.53[50]	0.427	0.853	0.581	0.649[a)]	0.849	0.423	0.500[a)]	0.664
RFB	0.375[51]	0.0188	0.0375	0.749	1.031[b)]	2.036	0.0851	0.199[b)]	0.636
STFX	1.000[52]	0.0500	0.100	0.0429	0.0555[a)]	0.0926	0.157	0.206[b)]	0.318
ZDV	1.100[53]	0.0550	0.110	3.17E-3	6.91E-3[a)]	0.0441	6.32E-4	1.97E-3[a)]	0.0601

[a)] Level 1/2 concentrations selected based on IC_{10}/IC_{20}; [b)] Level 1/2 concentrations selected based on 5%/10% C_{max}. Abbreviations: ARF, auranofin; ATS, artesunate; BLM, bleomycin; CPX, ciclopirox; FUDR, floxuridine; LVX, levofloxacin; MTF, metformin; MEM, meropenem; PMB, polymyxin B; RFB, rifabutin; STFX, sitafloxacin; ZDV, zidovudine.

both ENT646 and C31 isolates ($N = 8$) (Figure S2, Supporting Information). Most of the 155 OACD combinations resulted in non-inhibitory effects with only a few achieving maximal % Inhibition. The results suggest that simply pooling drugs in a cocktail does not always lead to the desired outcome. IDentif.AI correlated the % Inhibition values of all 155 combinations and their associated monotherapies. Box-Cox transformation evaluated the experimental data of both ENT646 and C31 isolates, and no transformation was determined. Subsequently, a suite of residual-based outlier analyses was performed for the % Inhibition data of each isolate, and no outliers were identified (Figure S3, Supporting Information). All data were included for the IDentif.AI analysis. IDentif.AI correlated the input combinations and their corresponding % Inhibition data via a second-order quadratic series, and the adjusted R^2 for ENT646 and C31 optimization were 0.853 and 0.726, respectively, indicating a highly correlated relationship between the input and output data. The resulting coefficients of the step-wise regression are summarized in Table S3 (Supporting Information). The analysis provided a ranked list of all possible combinations ($3^{12} = 531\,441$) based on the interpolation of the 155 OACD-designed combinations. The top-ranked 2-, 3-, and 4-drug combinations were selected for subsequent validation studies (**Table 2**). Interestingly, BLM/MEM combination consistently showed up as the top-ranked 2-drug combination in both ENT646 and C31 optimization. Furthermore, IDentif.AI's interaction analysis predicted potential strong synergy between BLM and MEM in both ENT646 and C31 isolates (Figure S4, Supporting Information). Aside from BLM/MEM, IDentif.AI also pointed to levofloxacin/sitafloxacin (LVX/STFX) as one of the top combinations against ENT646 isolate (Table 2), and interaction analysis also suggested synergistic interaction between the two drugs (Figure S4, Supporting Information).

The efficacies of the selected IDentif.AI-designed combinations were experimentally determined (Table 2). To provide a benchmark of the effectiveness of IDentif.AI-designed combinations, four standard-of-care (SOC) regimens were also validated. The concentrations of drugs in SOC regimens were determined in the same workflow as the original pool of 12 drugs (Figure S1 and Table S4, Supporting Information). All SOC drugs were tested at level 2 concentrations to ensure maximal efficacies. Among the four SOC combinations, only ceftazidime-avibactam (CAZ-AVI)/MEM demonstrated complete growth inhibition against ENT646 (100.07±0.06%) and C31 (100.02±0.13%), while the other three exhibited moderate (less than 50%) or minimal inhibitory efficacy against both strains (Table 2). Notably, IDentif.AI-designed BLM/MEM combination exhibited 92.12±7.77% Inhibition and 100.18±0.11/100.10±0.03% Inhibition (two different concentration ratios) against ENT646 and C31 isolates, respectively. Additionally, LVX/STFX, which is a double fluoroquinolone design, also exhibited maximal inhibitory effect (94.26±18.10/100.00±0.25% Inhibition against ENT646). No statistically significant efficacy difference ($p < 0.001$) was detected between CAZ-AVI/MEM and IDentif.AI-designed top combinations in both strains by Kruskal-Wallis and Dunn's post hoc tests.

Aside from pinpointing effective drug combinations, IDentif.AI also identifies ineffective ones formed by the same pool of drugs. In Table 2, a list of low-ranked ineffective combinations was also experimentally validated. In line with the IDentif.AI results, these combinations exhibited no inhibition. Therefore, properly pairing drugs in combinations is critical to achieving optimal outcomes.

2.3. Synergy Analysis and Activity Spectra Profiling of BLM/MEM and LVX/STFX

IDentif.AI interaction analysis predicted strong synergistic drug-drug interactions in BLM/MEM (against ENT646 and C31) and LVX/STFX (against ENT646) (Figure S4, Supporting Information). To validate the predicted synergy and to examine the activity spectra of the two combinations, checkerboard assays were performed in MHB against 9 clinical isolates from three key CRE species (*K. pneumoniae* ENT646/ENT448/ENT1192, *E. coli* C31/C165/C242, and *E. hormaechei* C36/C52/C254) (Table S1, Supporting Information). These whole-genome sequenced isolates possess genes coding for all three classes of carbapenemases, including Class A KPC (*K. pneumoniae* ENT646/ENT1192), Class B NDM (*K. pneumoniae* ENT448, *E. coli* C31/C242, *E. hormaechei* C52/C254), and Class C OXA (*K. pneumoniae* ENT646/ENT1192/ENT448, *E. coli* C165/C242, *E. hormaechei* C254). Moreover, both hypervirulent (ENT646, ENT1192) and classical (ENT448) *K. pneumoniae* isolates were tested. Drug gradients of BLM, MEM, LVX, and STFX were prepared at 2-fold serial dilutions starting at 20% C_{max}. % Inhibition efficacies were experimentally determined for each checkerboard assay, and they were fed into SynergyFinder+ for drug interaction analysis based on Bliss independence model. The model provided Bliss synergy δ-scores for each dose ratio across the checkerboard, and a score of >10 indicates the presence of synergy at the respective ratio. As shown in **Figure 2** and Figure S5 (Supporting Information), BLM/MEM combination exerted broad-spectrum antibacterial and strong synergistic effects against all tested isolates within the clinically actionable concentration ratios (≤10% C_{max}, dotted boxes). Analysis of dose-response curves of drugs in monotherapies and in combinations revealed potentiating interaction between BLM and MEM. For instance, BLM was found to significantly re-sensitize hv*Kp* ENT646/ENT1192 and *E. coli* C165 to the treatment of MEM, where high-level resistance was initially observed. Whereas in BLM-resistant strains, including *E. coli* C242 and *E. hormaechei* C36/C52/C254, MEM remarkably potentiated the potency of BLM. Moreover, classical *K. pneumoniae* (c*Kp*) ENT448 and *E. coli* C31, which showed complete resistance to both drugs when they were administered at indicated concentrations individually, became susceptible to the combination due to potentiation in both directions, and manifested Bliss Synergy δ-Scores of up to 90. In contrast, LVX/STFX combination only interacted synergistically against two hv*Kp* isolates (ENT646, ENT1192) (Figure S6, Supporting Information). This synergistic interaction is due to the potentiating effect of STFX to the activity of LVX against both strains (Figure S6, Supporting Information). Although MHB has been routinely used for antimicrobial susceptibility testing, it does not recapitulate the in vivo milieu. To examine BLM/MEM combination in a more clinically relevant setting, the checkerboard assays were repeated against the 9 CRE strains in M9 broth supplemented with 0.4% glucose, which has been reported to mimic the lung environment.[54] We found that BLM/MEM retains its antibacterial activity and strong synergistic interactions against all tested pathogens in M9 media (Figure S7, Supporting Information).

Table 2. Experimental validation of IDentif.AI-designed combinations with SOC regimens.

Strains	IDentif.AI-designed Combinations [$\mu g\ mL^{-1}$]	IDentif.AI Prediction		Experimental Validation
		Rank	% Inhibition	% Inhibition
ENT646	Top 2-drug Combinations			
	BLM (0.183)/MEM (1.283)	306 695	67.67	92.12±7.77
	LVX (0.607)/STFX (0.056)	330 869	64.04	94.26±18.10
	LVX (0.768)/STFX (0.056)	363 345	58.88	100.00±0.25
	Top 3-drug Combinations			
	BLM (0.183)/LVX (0.607)/MEM (1.283)	141 307	91.10	100.00±0.29
	BLM (0.183)/LVX (0.607)/STFX (0.056)	186 801	84.49	99.98±0.26
	BLM (0.183)/MEM (1.283)/ZDV (0.003)	194 073	83.48	88.24±10.68
	Top 4-drug Combinations			
	BLM (0.183)/LVX (0.607)/MEM (1.283)/STFX (0.056)	45 425	110.65	99.97±0.24
	BLM (0.183)/LVX (0.607)/MEM (1.283)/CPX (0.022)	51 713	108.86	99.92±0.18
	Low Ranked Ineffective Combinations			
	RFB (0.019)/STFX (0.043)	528 421	0.45	3.75±1.85
	ATS (0.165)/BLM (0.183)	525 894	5.85	7.10±1.30
	FUDR (0.013)/MTF (0.065)/PMB (0.581)	528 114	0.80	11.78±1.43
	ATS (0.165)/BLM (0.100)/CPX (0.022)	523 666	9.44	-0.34±1.84
	Standard-of-care (SOC) Combinations			
	CAZ-AVI (0.35)/MEM (1.283)	-	-	100.07±0.06
	CLT (0.092)/MEM (1.283)/TGC (0.045)	-	-	33.66±2.06
	ETM (3.123)/MEM (1.283)	-	-	10.95±1.39
	CLT (0.092)/ ETM (3.123)/MEM (1.283)	-	-	7.98±1.4
C31	Top 2-drug Combinations			
	BLM (50)/MEM (3.080)	151 780	74.62	100.18±0.11
	BLM (50)/MEM (6.160)	181 209	68.70	100.10±0.03
	BLM (50)/ZDV (0.002)	197 116	65.63	20.38±2.47
	Top 3-drug Combinations			
	BLM (50)/MEM (3.080)/ZDV (0.002)	51 802	99.53	100.02±0.06
	BLM (50)/MEM (3.080)/STFX (0.100)	68 300	94.50	100.21±0.14
	BLM (50)/LVX (0.930)/ZDV (0.002)	78 041	91.84	17.96±2.22
	Top 4-drug Combinations			
	BLM (100)/MEM (6.160)/LVX (0.930)/ZDV (0.002)	6400	125.73	100.20±0.08
	BLM (100)/MEM (6.160)/PMB (0.500)/STFX (0.100)	11 433	119.89	100.10±0.10
	Low Ranked Ineffective Combinations			
	ATS (0.330)/BLM (100)	526 923	-11.76	7.31±4.26
	ATS (0.165)/MEM (6.160)	525 117	-9.48	16.14±3.40
	BLM (100)/FUDR (0.026)/LVX (0.465)	525 751	-10.23	4.62±14.17
	ATS (0.165)/RFB (0.019)/ZDV (0.002)	526 224	-10.82	6.46±11.20
	Standard-of-care (SOC) Combinations			
	CAZ-AVI (23.97)/MEM (6.16)	-	-	100.02±0.13
	CLT (0.092)/MEM (6.16)/TGC (0.043)	-	-	23.02±2.4
	ETM (15.5)/MEM (6.16)	-	-	43.59±5.85
	CLT (0.092)/ ETM (15.5)/MEM (6.16)	-	-	18.33±2.43

Data points are presented as mean ± propagated SD (ENT646 N = 10, C31 N = 6). Abbreviations: CAZ-AVI, ceftazidime–avibactam; CLT, colistin; ETM, ertapenem; TGC, tigecycline.

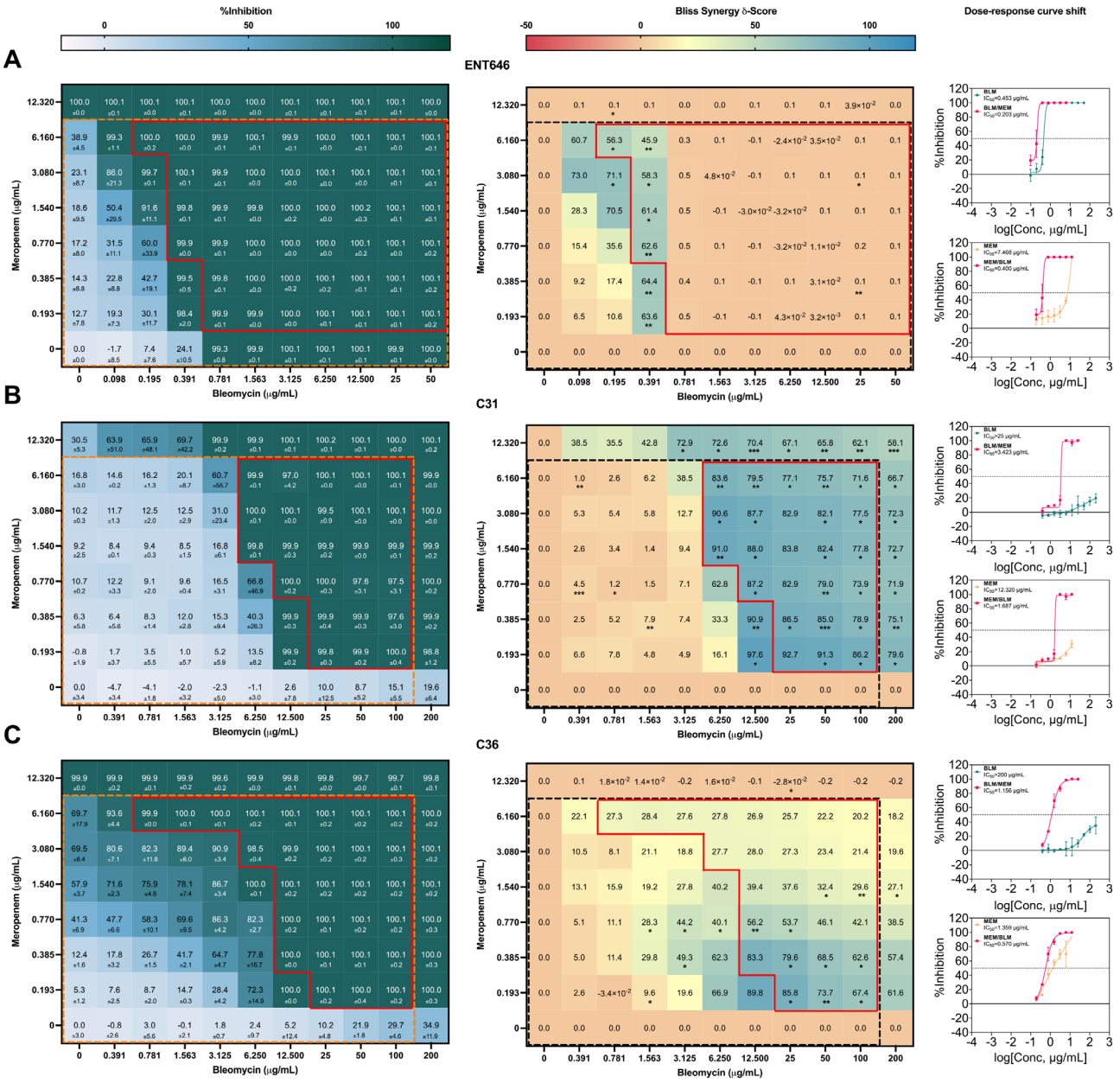

Figure 2. Drug interaction analysis of BLM/MEM against three clinical isolates from three key CRE species, respectively: A) hv*Kp* ENT646, B) *E. coli* C31, and C) *E. hormaechei* C36 in MHB. Drugs were tested starting from their 20% C_{max} concentrations or lower in 96-well plates. Clinically actionable concentration combinations (≤10% C_{max}) in each plate are boxed by dashed lines. Concentration ratios causing no less than 10 000-fold killing after 20 h incubation are boxed by red solid lines. Synergy was evaluated via the Bliss independence model. Synergy scores greater than 10, between −10 and 10, and less than −10 are considered synergistic, additive, and antagonistic, respectively. Statistical significance of the Bliss Synergy *δ*-Scores was determined by one-sample t-test (*$p < 0.05$; **$p < 0.01$; ***$p < 0.001$). The horizontal, black dotted line in each dose response curve plot represents absolute IC_{50}. Data points are presented as mean ± SD (N = 2).

2.4. Bactericidal Activity Testing and Spontaneous Resistance Propensity Evaluation of BLM/MEM

To assess the killing capacity of BLM/MEM at different concentration ratios, aliquots (100 μL) of cultures from wells of microtiter plates that showed 100% Inhibition were plated onto solid agar for colony-forming unit (CFU) enumeration. Concentration ratios in the checkerboard assays inducing more than 10 000-fold killing were screened and highlighted in red boxes on each interaction map. BLM/MEM at various concentration ratios potently killed all isolates tested in both rich (Figure 2 and Figure S5, Supporting Information) and minimal (Figure S7, Supporting Information) media. To profile the killing kinetic of BLM/MEM, mid-log-phase ENT646 and C31 cultured in MHB were exposed to BLM/MEM combination at different concentration ratios for 20 h. At each time point, culture aliquots

were adequately diluted and plated for CFU counting. A range of BLM/MEM concentration ratios were tested including the minimum concentration ratios defined from the checkerboard assays showing both synergistic (Bliss Synergy δ-Score > 10) and bactericidal (≥10 000-fold killing) effects, and the concentration ratios used for IDentif.AI analysis. To provide a benchmark, CAZ-AVI/MEM, the only effective SOC combination, was also tested at level 2 concentrations. The positive control CAZ-AVI/MEM rapidly and thoroughly killed both ENT646 and C31 within 20 h (Figure S8, Supporting Information). Its killing activity was particularly robust against *E. coli* C31 with no viable bacteria detected (CFU < 20) at time point as early as 5 h. In comparison to CAZ-AVI/MEM, all tested concentration ratios of BLM/MEM exhibit similar or even better killing kinetics against the treated cultures. The only exception is BLM (0.183 μg mL^{-1})/MEM (1.283 μg mL^{-1}) against ENT646, which only killed bacteria at early time points (within 5 h), then the CFU increase to the inoculum level by the end of the treatment (20 h). The regrowth of CFU in the treated culture could be due to the instability and gradual loss of efficacy of MEM incubated at 37 °C.[55] It is unlikely due to the emergence of resistant bacteria, as the regrown culture demonstrated similar growth as compared to the initial culture when treated with BLM/MEM at the same concentration ratio (0.183 μg mL^{-1}/1.283 μg mL^{-1}) (data not shown). In fact, we found that BLM/MEM has a low propensity for the selection of spontaneous resistant mutants (<10^{-9}/CFU mutation frequency).

2.5. Synergistic Interactions of BLM with Other Carbapenems

Carbapenems constitute an essential component in the combinatorial regimens against CRE infections. The observed strong synergism in BLM/MEM prompts us to ask whether synergism exists between BLM with other carbapenems. Ertapenem (ETM) and imipenem (IMP) are two commonly administered carbapenems in clinics. Checkerboard assay followed by CFU enumeration was repeated for BLM/ETM and BLM/IMP against both hv*Kp* ENT646 and *E. coli* C31 in MHB. As shown in Figure S9 (Supporting Information), the strong synergy of BLM/MEM observed in ENT646 and C31 extended to ETM and IMP. Within clinically actionable concentrations (≤10% C_{max}, dotted boxes), BLM/ETM and BLM/IMP were also found to be bactericidal at multiple concentration ratios (red solid boxes). The dose-response analysis revealed similar drug interaction patterns to BLM/MEM, where BLM potentiated the efficacy of tested carbapenems in ENT646, while against C31 bidirectional potency enhancements were evidenced. Therefore, BLM may potentially synergize with most carbapenems. However, BLM/MEM remains the most promising among the three tested (BLM/MEM, BLM/ETM, BLM/IMP), demonstrating the strongest synergism and the highest bactericidal activity at lower doses.

2.6. Cytotoxicity Assessment of BLM/MEM Against Two Different Cell Lines

Anti-cancer drug BLM is notorious for genotoxicity and side effects.[56] To investigate whether cytotoxicity in mammalian cells was also enhanced due to the drug-drug interplay, the liver HepG2 and macrophage THP1 cell-lines were cultured and exposed to BLM/MEM treatment. BLM and MEM were both tested from their 20% C_{max} concentrations (BLM: 200 μg mL^{-1}, MEM: 12.32 μg mL^{-1}) and treatments were performed for short (24 h) and long (72 h) durations (**Figure 3**). In the first 24 h, no cytotoxicity was detected for both cell lines within clinically relevant concentrations (≤10% C_{max}, black dotted boxes). More than 50% cytotoxicity was only seen in HepG2 cells after prolonged combinatorial treatment (72 h) with BLM administered at higher concentrations (>25 μg mL^{-1}, 2.5% C_{max}). Moreover, cytotoxicity-induced synergistic interaction was not observed in either cell line throughout the treatment duration, indicating that the potentiating effects between BLM and MEM are only seen in bacteria (Figure 3). Even though toxicity is a major concern regarding the use of BLM for treating bacterial infections, the synergistic interactions of BLM/MEM substantially decrease the necessary dose of BLM to achieve maximal antibacterial effects, thus mitigating toxicity. It is important to note that the BLM/MEM combination with BLM at 2.5% C_{max} (25 μg mL^{-1}) synergistically killed eight pathogens out of the nine tested in MHB (Figure 2 and Figure S5, Supporting Information) and all nine pathogens in M9+0.4% glucose (Figure S7, Supporting Information). The only exception is c*Kp* ENT448 in MHB, in which bactericidal dose ratios were composed of BLM at its 2.5% C_{max} or higher concentrations (Figure S5, Supporting Information).

3. Discussion

Carbapenem-resistant *Enterobacteriaceae* causes life-threatening infections and high mortality due to its resistance to nearly all antibiotics. Therefore, anti-CRE combinatorial treatments must move beyond the traditional antibiotics and towards the huge pool of repurposed drugs already in market. IDentif.AI is positioned as a novel digital medicine and pandemic readiness platform to meet the challenges of a huge parameter space resulting from drug and dose selections. It efficiently optimizes regimens by testing a minimal set of combinations, 155 out of half a million combinations (3^{12} = 531 441). In this study, through the utilization of IDentif.AI, BLM/MEM was independently identified against both the hypervirulent *K. pneumoniae* strain ENT646 as well as the *E. coli* C31 strain, demonstrating broad-spectrum synergism and bactericidal activity. The efficacy is retained in M9 minimal medium that is more reflective of in vivo niches than rich medium, and no resistance mutants were detected. BLM also synergized with IMP and ETM, which further unveiled common synergism that could exist between BLM and other carbapenem antibiotics. The mechanism underlying this synergy remains to be investigated. Taken together, our data suggest BLM/MEM as an alternative drug combination for the treatment of severe CRE infections. Although BLM toxicity could be a concern hindering the future clinical use of BLM/MEM, our data on THP1 and HepG2 cell-lines detected no cytotoxicity at clinically relevant concentrations (≤ 10% C_{max}) within 24 h. Higher than 50% significant cytotoxicity was restricted to HepG2 cells treated for a prolonged time of 3 days at BLM concentrations higher than its 2.5% C_{max}. BLM/MEM with BLM doses lower than 2.5% C_{max} was still synergistically active against 17 culture conditions out of the 18 tested (9 isolates in two media types), giving a more

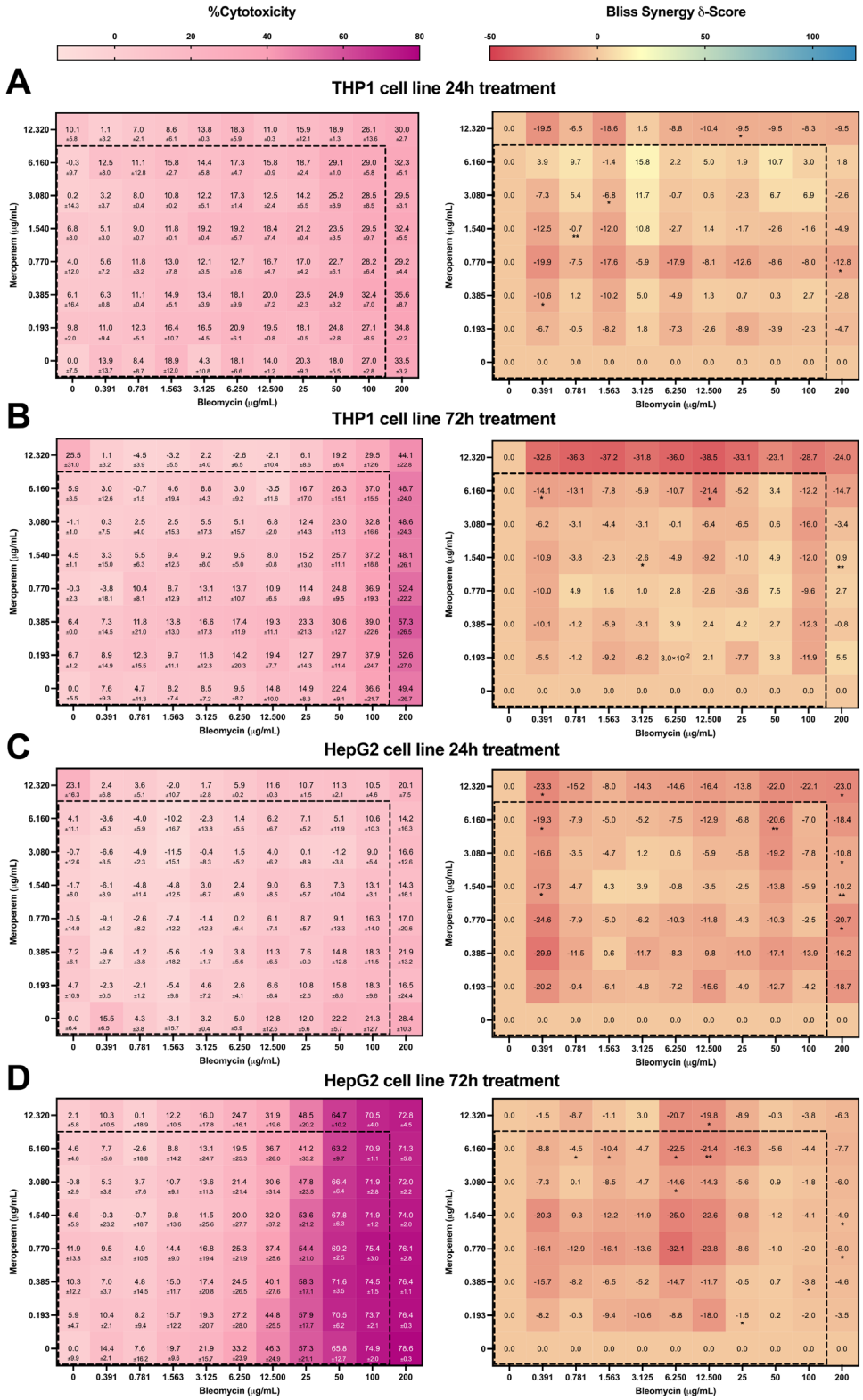

Figure 3. Cytotoxicity analysis of BLM/MEM. A) THP1 after 24 h treatment and B) 72 h treatment. C) HepG2 after 24 h treatment and D) 72 h treatment. Synergy in cytotoxicity was evaluated by the Bliss independence model, scores greater than 10, between −10 and 10, and less than −10 implicates synergistic, additive, and antagonistic interaction, respectively. Statistical significance of the Bliss Synergy δ-Scores was determined by one-sample t-test (*$p < 0.05$; **$p < 0.01$; ***$p < 0.001$). The clinically actionable concentration ranges are boxed in black dotted lines (≤ 10% C_{max}). Data points are presented as mean ± SD (N = 2).

than 94% effectiveness coverage. This coverage rate could be further defined by exposing more clinical isolates to the treatment of BLM/MEM under varied conditions. Even though the pairing of MEM with BLM remarkably enhanced the resultant antibacterial potency, no synergism in mammalian cytotoxicity was observed. BLM/MEM could be very useful in treating pneumonia, one of the most common infections caused by CRE pathogens, because BLM preferentially accumulates in the lungs.[56] However, it is important to realize that all results reported in this study are based on in vitro validations. Further preclinical studies including animal models are needed to assess the clinical suitability and safety of the combination. BLM/MEM can only be considered optimal within the tested pool of drugs, and experimenting with a different set of drugs may yield other actionable drug combinations. Nonetheless, we uncovered an unexpected and novel combination that would not have been discovered otherwise.

Recently, an outbreak of *K. pneumoniae* was reported by the Virginia Mason Franciscan Health. Virginia Mason Medical Center detected multiple transmissions of an unknown strain of *K. pneumoniae*, and has reported 31 confirmed infections. The most recent infection was confirmed on April 3, 2023 and importantly, 7 infected patients have passed away since October 2022. The source of this specific strain is unknown.[57] The development of a diverse range of anti-CRE treatment options should be prioritized. IDentif.AI may play a critical role in future incidences like the above-mentioned outbreak. The same optimization workflow outlined in this study may rapidly determine an appropriate regimen upon isolating the strain of *K. pneumoniae* from the infected patients. Moreover, clinical input for the initial selection of drugs and accounting for pharmacological data in the workflow of IDentif.AI contributes to the potential success of clinical translation of IDentif.AI-designed combinations. More importantly, IDentif.AI may further personalize the optimal regimen for each infected patient using individually obtained strains of the bacteria. In sum, this platform may be a powerful tool that can potentially recommend effective treatment options during a sudden outbreak as the workflow only requires minimal experimentation and short timeline. Though IDentif.AI is a versatile, dynamic platform, it also has some technical limitations. Notably, IDentif.AI relies on the AI-derived second-order quadratic relationship that correlates input combinations with their corresponding biological response. This relationship therefore limits the number of drugs for interaction analysis. For example, IDentif.AI interaction analysis including the estimated coefficients (Figure S4 and Table S3, Supporting Information) was mostly limited to 2-drug combinations. Incorporating higher-order drug optimization and/or pairing with high-throughput screening may potentially enable detailed analyses of drug combinations containing more drugs. Moreover, the OACD utilized in this experiment only contained three concentration levels. The level 1 and level 2 concentrations may not cover a wide range of concentrations and as a result, some drug-drug interactions may be missed. Therefore, an experimental design that can incorporate more concentration levels while maintaining a manageable experimental setup may potentially lead to the detection of more drug interactions.

The emergence of digital medicine has led to the application of artificial intelligence in addressing healthcare challenges including AMR. In a study by Chen et al., statistical metamodeling was harnessed to determine synergistic antimicrobial interactions in *E. coli*.[58] Similar to IDentif.AI, this approach also utilizes fractional factorial followed by stepwise regression for pinpointing actionable drug combinations. However, IDentif.AI uses OACD, which includes fractional factorial and orthogonal array, for its initial drug screening. As a result, both linear and non-linear (quadratic) effects were considered, while statistical metamodeling explores the two effects separately. In addition, higher-order drug interactions are also being explored aside from conventional pair-wise drug interactions. A recent study reported that when more drugs are added to the bacterium's environment, the prevalence of higher-order drug interactions increases.[59] IDentif.AI harnesses a second-order quadratic series that provides insights into interactions between two drugs, as higher-order drug combinations may not be as clinically relevant as 2- or 3-drug combinations. The integration of various different drug combination optimization approaches may lead to more actionable outcomes.

In summary, by harnessing the IDentif.AI platform, we identified BLM/MEM to be an important combinatorial alternative should preclinical and clinical testing show favorable safety and efficacy profiles for use in patients with CRE infections with very limited therapeutic options. Our work demonstrates the utility of the IDentif.AI platform and validates the accuracy of its prediction on top-ranked effective combinations. Subjecting strains from distinct species to the IDentif.AI platform in parallel could be a feasible strategy for the discovery of pan-active combinations against a family of bacteria. In the future, integrating IDentif.AI with current drug development pipeline could be an important advancement made to shorten regimen composition duration and to increase treatment success rates.

4. Conclusion

This study presents an alternative approach to accelerate the development of CRE-specific treatment strategies and potentially enrich our arsenal of treatment options in the face of surging antimicrobial resistance. IDentif.AI-pinpointed BLM/MEM combination demonstrated promising results in vitro against multiple species of CRE. However, further validations including in vivo and preclinical studies may be helpful in clinical translation. Nonetheless, the platform and the combinations may contribute to future pandemic readiness and the accessibility of treatment options for the clinical communities.

5. Experimental Section

Bacterial Strains and Culture Conditions: A total of nine carbapenem-resistant *Enterobacteriaceae* (CRE) clinical isolates were tested in this study, namely *Klebsiella pneumoniae* ENT646/ENT1192/ENT448.[38] *Escherichia coli* C31/C165/C242, and *Enterobacter hormaechei* C36/C52/C254. Hypervirulent (ENT646, ENT1192) and classical (ENT448) *K. pneumoniae* strains were obtained from the Carbapenemase-producing *Enterobacteriaceae* in Singapore (CaPES).[60] *E. coli* and *E. hormaechei* strains were from the National University Hospital. Bacterial cultures were maintained at 37°C in Mueller Hinton Broth (MHB) (BD Difco). To test drug combinations in minimal media, M9 media supplemented with 0.4% glucose was prepared by diluting M9 minimal salts at 5× (Sigma) to 1× in ddH_2O containing 2 mM $MgSO_4$, 100 μM

$CaCl_2$, and 0.4% glucose. Genomic DNAs of *E. coli* and *E. hormaechei* strains were extracted following the GenElute Bacterial Genomic DNA Kit Protocol (Sigma) and sequenced on a NovaSeq PE150 sequencing platform by NovogeneAIT. Genomic sequences were uploaded to NCBI with accession numbers indicated in Table S1 (Supporting Information). To identify resistance genes, bacterial genome sequence data were uploaded to CARD (The Comprehensive Antibiotic Resistance Database).

Selection and Stock Preparation of Drugs: Twelve FDA-approved drugs with diverse clinical indications were selected through a comprehensive literature review. Bleomycin (BLM) (SelleckChem S1214), floxuridine (FUDR) (SelleckChem S1299), metformin (MTF) (SelleckChem S5958), meropenem (MEM) (SelleckChem S1381), and polymyxin B (PMB) (SelleckChem S1395) were dissolved in sterile ddH_2O. Auranofin (ARF) (SelleckChem S4307), artesunate (ATS) (SelleckChem S2265), ciclopirox (CPX) (SelleckChem S2528), levofloxacin (LVX) (SelleckChem S1940), rifabutin (RFB) (SelleckChem S1741), sitafloxacin (STFX) (SelleckChem S2152), and zidovudine (ZDV) (SelleckChem S2579) were prepared in DMSO. Drugs commonly administered in clinics against CRE infections were tested as standard-of-care (SOC) agents, including ceftazidime-avibactam (CAZ-AVI at 4:1 dose ratio) (MedChemExpress HY-B0593/HY-14879A), colistin (CLT) (SelleckChem S4029), tigecycline (TGC) (MedChemExpress, HY-B0117), ertapenem (ETM) (MedChemExpress, HY-13625), and MEM. ETM and TGC were dissolved in DMSO, and the remaining SOC drugs were prepared in sterile ddH_2O. All drug stocks were aliquoted and kept at −20 °C.

Dose-Response Curve Determination: Minimum inhibitory concentration (MIC) assay was conducted to profile the dose-response curves of the 12 selected drugs and SOC drugs against ENT646 and C31, following the Clinical and Laboratory Standards Institute guidelines (CLSI-M07-A11-2018). Briefly, 100 µL of bacterial inoculum at 1×10^6 CFU mL^{-1} (OD_{600} 0.001) were dispensed into each well of flat-bottomed transparent 96-well microplates (Greiner) containing 100 µL of twofold serially diluted drug gradients. OD_{600} readings were recorded on a Tecan Infinite M200 PRO plate reader before and after incubation at 37 °C for 20 h without shaking. Growth of bacteria ($OD_{600\ growth}$) in each well of the microplate was obtained by subtracting the OD_{600} reading at time zero from that after incubation. % Inhibition was calculated using Equation (1):

$$\%\ \text{Inhibition} = \left[1 - \left(\frac{OD_{600\ growth}\ \text{in drug treated well}}{OD_{600\ growth}\ \text{in drug free well}}\right)\right] \times 100 \quad (1)$$

To construct dose-response curves, the logarithmic scale of drug concentration was plotted against the measured % inhibitions on GraphPad PRISM (GraphPad Software). Based on the plotted dose-response curves, IC_{10}, IC_{20}, and IC_{50}, minimum drug concentrations achieving 10%, 20%, and 50% inhibition of bacterial growth, respectively, were obtained. Across all experiments, drug-free (DF) wells were used as negative controls. The final concentration of DMSO in each well was kept below 0.5%. Experiments were repeated by at least two independent biological replicates, each of which contains 4 technical replicates.

IDentif.AI Interrogated Drug Combinations and Interactions: A resolution 5.5 orthogonal array composite design (OACD)[61,62] consisting of 128-combination two-level fractional factorial and 27-combination three-level orthogonal array (Table S2, Supporting Information). All 155 OACD combinations were experimentally prepared and validated for both ENT646 and C31 strains (N = 3). The monotherapies of all 12 drugs in two concentration levels were also validated. IDentif.AI correlated the input combinations including the monotherapies to their respective measured % Inhibition via a second-order quadratic series.[16,27–29] Box-Cox transformation evaluated the % Inhibition data to determine the most suitable data transformation that may enhance the goodness-of-fit of the regression analysis. Residual-based outlier analysis was also performed. Subsequently, IDentif.AI performed a stepwise regression to interrogate and pinpoint top combinations from a search space of 12 drugs at three concentration levels, which consists of (3^{12}) 531 441 possible combinations. IDentif.AI provided a ranked list of all possible combinations containing their respective concentrations and IDentif.AI-predicted % Inhibition. IDentfi.AI was performed on MATLAB (R2020B; MathWorks, Inc).

Checkerboard Assay with Bliss Independence Model Synergy Analysis: Serial twofold dilutions of interested two drugs were prepared and combined in vertical directions in 96-well plates. One hundred microliters of bacterial suspension at 1×10^6 CFU mL^{-1} (OD_{600} 0.001) was added. Plates were incubated at 37 °C without shaking for 20 h. OD_{600} readings were recorded before and after incubation. % Inhibition was determined for each concentration ratio to generate interaction maps. % Inhibition data were subsequently uploaded to SynergyFinder+ and analyzed by the Bliss independence model.[60] The resulting synergy scores for all combinations were plotted. Dose-response curves were also plotted to compare each combination and corresponding monotherapies. All graphs were generated on GraphPad PRISM (GraphPad Software). Experiments were done in both MHB and M9+0.4% glucose media ($N = 2$).

Bactericidal Activity Determination from 96-Well Checkerboard Microplates: To detect the bactericidal activity of combinations (BLM/MEM, BLM/ETM, BLM/IPM) at different dose ratios, 100 µL of neat bacterial cultures were aliquoted from wells of microplates showing no detectable bacterial growth by end of the checkerboard titration assay and plated out onto LB agar for colony forming unit (CFU) enumeration. Wells inducing at least 10 000-fold bacterial death as compared to the initial inoculum CFU were indicated on the plates. The experiment was repeated at least twice.

Time-Kill Kinetics Analysis: Bacterial suspensions of ENT646 and C31 at 5×10^5 CFU mL^{-1} (OD_{600} 0.0005) were prepared in MHB and treated with combinations at interested concentrations for 20 h at 37 °C with shaking. At each indicated time point (0, 0.5, 1, 3, 5, and 20 h), cultures were aliquoted and serially diluted in MHB. Fifty microliters of diluted or neat bacterial samples were plated onto LB agar. After overnight incubation at 37 °C, colonies on the LB agar were counted and the $\log_{10}$ CFU mL^{-1} was plotted against the time course to obtain the time-kill kinetic curves. The experiment was repeated thrice.

Spontaneous Mutant Selection: To evaluate the spontaneous resistance frequency associated with BLM/MEM combination treatment, *E. coli* C31 showing resistance to both BLM and MEM when drugs were administered alone was utilized following a reported method with modifications.[61] Briefly, 10^8 and 10^9 of C31 cells at mid-log phase (OD_{600} 0.4–0.6) in MHB were plated onto LB agar containing BLM/MEM at varied bactericidal concentrations: 100 µg mL^{-1}/6.16 µg mL^{-1}, 50 µg mL^{-1}/3.08 µg mL^{-1}, 25 µg mL^{-1}/1.54 µg mL^{-1}, and 12.5 µg mL^{-1}/0.77 µg mL^{-1}. Plates were incubated at 37 °C overnight (MEM gradually loses its activity when incubated at 37 °C for a longer time than 24 h.[55] Any singly isolated colonies appearing on the agar were re-streaked onto freshly prepared agar containing the same concentration of combinations. Two independent biological experiments were performed.

Cytotoxicity Test: Cytotoxicity was measured on macrophage THP1 and liver HepG2 cell lines following a standard MTT (3-(4,5-dimethylthiazol-2-yl)−2,5-diphenyltetrazolium bromide) (Sigma) Cell Viability Assay.[62] Briefly, THP1 and HepG2 cells were cultured in complete Roswell Park Memorial Institute (RPMI) 1640 medium and Dulbecco's Modified Eagle Medium (DMEM) (Gibco) supplemented with 10% fetal bovine serum (FBS) (HyClone) and 1% penicillin-streptomycin (100×) (Biowest), respectively. 1×10^5 THP1 cells treated with 100 ng mL^{-1} phorbol 12-myristate 13-acetate (PMA) (Sigma) (or 2×10^4 HepG2 cells) were seeded in each well of flat-bottomed 96-well microplates (Greiner). After 24 h at 37 °C with 5% CO_2, the medium in each well was replaced with 100 µL RPMI+10% FBS (or DMEM+10% FBS) containing BLM/MEM at varied concentrations in the checkerboard format. Both BLM and MEM were tested starting from their 20% C_{max} concentrations. Cells were treated with drug combinations for 24 or 72 h. After that, medium-containing drugs were removed and 50 µL of freshly prepared MTT solution at 1 mg mL^{-1} in colorless Minimum Essential Medium (Gibco) were added into each well of the microplates. Plates were incubated for 2 h at 37 °C for the generation of formazan which were eventually dissolved in 100 µL 100% isopropanol (Fisher Chemical)

and detected at 570 nm on a Tecan Infinite M200 PRO plate reader. % Cytotoxicity was calculated using Equation (2):

$$\%\ \text{Cytotoxicity} = \left[1 - \left(\frac{\text{OD}_{570}\ \text{in drug treated wells}}{\text{OD}_{570}\ \text{in drug free wells}}\right)\right] \times 100 \quad (2)$$

Statistical Analysis: All in vitro experiments were performed in at least three biological replicates, except for the checkerboards, which only had two biological replicates. Experimentally derived data are presented as mean ± propagated SD for data in which biological replicates were performed within the same week (Equation S1, Supporting Information). However, biological replicates that were performed at different timepoints due to BLM shortages are presented as mean ± SD, arising from the replicates. This was mainly due to MIC shifts in replicates (both treated and controls) that were performed at different timepoints. The IDentif.AI analysis and its estimated coefficients were analyzed using sum of square *F*-test. The *p*-values of IDentif.AI-estimated coefficients served as coefficient exclusion criteria for stepwise regression (Table S3, Supporting Information). The distribution of the % Inhibition data for experimentally validated combinations was tested using the Shapiro–Wilk normality test. For multiple comparison and pairwise comparison, Kruskal–Wallis test and Dunn's post hoc test were performed, respectively. The statistical significance of synergy scores obtained via Bliss independence model was determined using one-sample *t*-test.

Supporting Information

Supporting Information is available from the Wiley Online Library or from the author.

Acknowledgements

This work is funded by grants NMRC OFIRG23jan-0060 and MOE2018-T3-1-003 to YH Gan.

Conflict of Interest

The authors declare no conflict of interest.

Author Contributions

M.L., K.Y., and P.W. contributed equally to this work and are joint first authors. M.L., L.H., and S.A.Q carried out in vitro experiments. M.L., K.Y., P.W., A.B., E.K.-H.C., D.H., and Y.H.G. conceptualized this work. C.Y.H. assisted in genome sequence data analysis. S.B.T. assisted in data analysis. J.T., O.T.N., K.M., and I.V. provided clinical isolates for testing. A.B., E.K.-H.C., D.H., and Y.H.G. provided insights and guidance throughout the study. M.L., K.Y., P.W., and Y.H.G. contributed to the writing of the manuscript. Review and editing were performed by all authors.

Data Availability Statement

The data that support the findings of this study are available in the supplementary material of this article.

Keywords

artificial intelligence (AI), carbapenem resistance, combination therapies, Enterobacteriaceae

Received: September 15, 2023
Revised: January 5, 2024
Published online: January 18, 2024

[1] S. Reardon, *Nature* **2014**, *15*, 135.
[2] P. Dadgostar, *Infect Drug Resist* **2019**, 3903.
[3] E. Tacconelli, E. Carrara, A. Savoldi, S. Harbarth, M. Mendelson, D. L. Monnet, C. Pulcini, G. Kahlmeter, J. Kluytmans, Y. Carmeli, M. Ouellette, K. Outterson, J. Patel, M. Cavaleri, E. M. Cox, C. R. Houchens, M. L. Grayson, P. Hansen, N. Singh, U. Theuretzbacher, N. Magrini, A. O. Aboderin, S. S. Al-Abri, N. Awang Jalil, N. Benzonana, S. Bhattacharya, A. J. Brink, F. R. Burkert, O. Cars, G. Cornaglia, et al., *Lancet Infect. Dis.* **2018**, *18*, 318.
[4] H.-J. Tang, C.-F. Hsieh, P.-C. Chang, J.-J. Chen, Y.-H. Lin, C.-C. Lai, C.-M. Chao, Y.-C. Chuang, *PLoS One* **2016**, *11*, 0151897.
[5] J. T. Jacob, E. Klein, R. Laxminarayan, Z. Beldavs, R. Lynfield, A. J. Kallen, P. Ricks, J. Edwards, A. Srinivasan, S. Fridkin, *Morb. Mortal. Wkly. Rep.* **2013**, *62*, 165.
[6] M. Tumbarello, P. Viale, C. Viscoli, E. M. Trecarichi, F. Tumietto, A. Marchese, T. Spanu, S. Ambretti, F. Ginocchio, F. Cristini, A. R. Losito, S. Tedeschi, R. Cauda, M. Bassetti, *Clin. Infect. Dis.* **2012**, *55*, 943.
[7] R. R. T. S. Investigators, *N. Engl. J. Med.* **2009**, *361*, 1627.
[8] N. Petrosillo, M. Giannella, R. Lewis, P. Viale, *Expert Rev. Anti-Infect. Ther.* **2013**, *11*, 159.
[9] L. S. Tzouvelekis, A. Markogiannakis, E. Piperaki, M. Souli, G. L. Daikos, *Clin. Microbiol. Infect.* **2014**, *20*, 862.
[10] J. F. Camargo, J. Simkins, T. Beduschi, A. Tekin, L. Aragon, A. Pérez-Cardona, C. E. Prado, M. I. Morris, L. M. Abbo, R. Cantón, *Antimicrob. Agents Chemother. 59*, 5903.
[11] C. Zhu, Q. Yang, L. Liu, S. Wang, *Angew. Chem., Int. Ed.* **2011**, *50*, 9607.
[12] X. Liu, R. E. Painter, K. Enesa, D. Holmes, G. Whyte, C. G. Garlisi, F. J. Monsma, M. Rehak, F. F. Craig, C. A. Smith, *Lab Chip* **2016**, *16*, 1636.
[13] J. Lv, S. Deng, L. Zhang, *Biosaf Health* **2021**, *3*, 22.
[14] U. Fanelli, M. Pappalardo, V. Chinè, P. Gismondi, C. Neglia, A. Argentiero, A. Calderaro, A. Prati, S. Esposito, *Antibiotics* **2020**, *9*, 767.
[15] I. Al-Shyoukh, F. Yu, J. Feng, K. Yan, S. Dubinett, C.-M. Ho, J. S. Shamma, R. Sun, *BMC Syst. Biol.* **2011**, *5*, 88.
[16] A. Blasiak, A. T. L. Truong, A. Remus, L. Hooi, S. G. K. Seah, P. Wang, D. H. Chye, A. P. C. Lim, K. T. Ng, S. T. Teo, Y.-J. Tan, D. M. Allen, L. Y. A. Chai, W. J. Chng, R. T. P. Lin, D. C. B. Lye, J. E.-L. Wong, G.-Y. G. Tan, C. E. Z. Chan, E. K.-H. Chow, D. Ho, *NPJ Digit Med* **2022**, *5*, 83.
[17] Q. Liu, C. Zhang, X. Ding, H. Deng, D. Zhang, W. Cui, H. Xu, Y. Wang, W. Xu, L. Lv, H. Zhang, Y. He, Q. Wu, M. Szyf, C.-M. Ho, J. Zhu, *Sci. Rep.* **2015**, *5*, 11464.
[18] D. L. Clemens, B.-Y. Lee, A. Silva, B. J. Dillon, S. Maslesa-Galic, S. Nava, X. Ding, C.-M. Ho, M. A. Horwitz, *PLoS One* **2019**, *14*, e0215607.
[19] S. De Mel, M. B. M. Rashid, X. Y. Zhang, J. Goh, C. T. Lee, L. M. Poon, E. H. L. Chan, X. Liu, W. J. Chng, Y. L. Chee, J. Lee, Y. C. Yuen, J. Q. Lim, B. K. H. Chia, Y. Laurensia, D. Huang, W. L. Pang, D. M. Z. Cheah, E. K. Y. Wong, C. K. Ong, T. Tang, S. T. Lim, S. B. Ng, S. Y. Tan, H.-Y. Loi, L. K. Tan, E. K. Chow, A. D. Jeyasekharan, *Blood Cancer J* **2020**, *10*, 9.
[20] B.-Y. Lee, D. L. Clemens, A. Silva, B. J. Dillon, S. Maslesa-Galic, S. Nava, X. Ding, C.-M. Ho, M. A. Horwitz, *Nat. Commun.* **2017**, *8*, 14183.
[21] M. B. Mohd Abdul Rashid, T. B. Toh, A. Silva, L. Nurrul Abdullah, C.-M. Ho, D. Ho, E. K.-H. Chow, *J Lab Autom* **2015**, *20*, 423.
[22] M. B. M. A. Rashid, T. B. Toh, L. Hooi, A. Silva, Y. Zhang, P. F. Tan, A. L. Teh, N. Karnani, S. Jha, C.-M. Ho, W. J. Chng, D. Ho, E. K.-H. Chow, *Sci. Transl. Med.* **2018**, *10*, eaan0941.
[23] Y. Shen, T. Liu, J. Chen, X. Li, L. Liu, J. Shen, J. Wang, R. Zhang, M. Sun, Z. Wang, W. Song, T. Qi, Y. Tang, X. Meng, L. Zhang, D. Ho, C.-M. Ho, X. Ding, H.-Z. Lu, *Adv. Therap.* **2020**, *3*, 1900114.
[24] A. Silva, B.-Y. Lee, D. L. Clemens, T. Kee, X. Ding, C.-M. Ho, M. A. Horwitz, *Proc. Natl. Acad. Sci. USA* **2016**, *113*, E2172.
[25] H. Wang, D.-K. Lee, K.-Y. Chen, J.-Y. Chen, K. Zhang, A. Silva, C.-M. Ho, D. Ho, *ACS Nano* **2015**, *9*, 3332.

[26] P. K. Wong, F. Yu, A. Shahangian, G. Cheng, R. Sun, C.-M. Ho, *Proc. Natl. Acad. Sci. USA* **2008**, *105*, 5105.
[27] A. Blasiak, J. J. Lim, S. G. K. Seah, T. Kee, A. Remus, D. H. Chye, P. S. Wong, L. Hooi, A. T. L. Truong, N. Le, C. E. Z. Chan, R. Desai, X. Ding, B. J. Hanson, E. K.-H. Chow, D. Ho, *Bioeng. Transl. Med.* **2021**, *6*, e10196.
[28] A. Blasiak, A. T. L. Truong, P. Wang, L. Hooi, D. H. Chye, S.-B. Tan, K. You, A. Remus, D. M. Allen, L. Y. A. Chai, C. E. Z. Chan, D. C. B. Lye, G.-Y. G. Tan, S. G. K. Seah, E. K.-H. Chow, D. Ho, *ACS Nano* **2022**, *16*, 15141.
[29] D. Mukherjee, P. Wang, L. Hooi, V. Sandhu, K. You, A. Blasiak, E. K.-H. Chow, D. Ho, P. L. R. Ee, *Theranostics* **2022**, *12*, 6848.
[30] Y. Honda, X. Ding, F. Mussano, A. Wiberg, C. Ho, I. Nishimura, in 2011 International Symposium on Micro-NanoMechatronics and Human Science **2011**, 4.
[31] B. K. J. Tan, C. B. Teo, X. Tadeo, S. Peng, H. P. L. Soh, S. D. X. Du, V. W. Y. Luo, A. Bandla, R. Sundar, D. Ho, T. W. Kee, A. Blasiak, *Front Digit Health* **2021**, *3*, 635524.
[32] T. Kee, C. Weiyan, A. Blasiak, P. Wang, J. K. Chong, J. Chen, B. T. T. Yeo, D. Ho, C. L. Asplund, *Adv. Therap.* **2019**, *2*, 1900023.
[33] A. J. Pantuck, D.-K. Lee, T. Kee, P. Wang, S. Lakhotia, M. H. Silverman, C. Mathis, A. Drakaki, A. S. Belldegrun, C.-M. Ho, D. Ho, *Adv. Therap.* **2018**, *1*, 1800104.
[34] A. Zarrinpar, D.-K. Lee, A. Silva, N. Datta, T. Kee, C. Eriksen, K. Weigle, V. Agopian, F. Kaldas, D. Farmer, S. E. Wang, R. Busuttil, C.-M. Ho, D. Ho, *Sci. Transl. Med.* **2016**, *8*, 333ra49.
[35] A. Blasiak, J. Khong, T. Kee, *SLAS TECHNOLOGY: Translating Life Sciences Innovation* **2020**, *25*, 95.
[36] D. Ho, P. Wang, T. Kee, *Nanoscale Horiz.* **2019**, *4*, 365.
[37] K. You, P. Wang, D. Ho, *Front Digit Health* **2022**, *4*, 830656.
[38] Y. Chen, K. Marimuthu, J. Teo, I. Venkatachalam, B. P. Z. Cherng, L. De Wang, S. R. S. Prakki, W. Xu, Y. H. Tan, L. C. Nguyen, T. H. Koh, O. T. Ng, Y.-H. Gan, *Emerg Infect Dis* **2020**, *26*, 549.
[39] R. Zhang, D. Lin, E. W.-C. Chan, D. Gu, G.-X. Chen, S. Chen, *Antimicrob. Agents Chemother.* **2016**, *60*, 709.
[40] X. Yang, N. Dong, E. W.-C. Chan, R. Zhang, S. Chen, *Trends Microbiol.* **2021**, *29*, 65.
[41] D. Van Duin, K. S. Kaye, E. A. Neuner, R. A. Bonomo, *Diagn. Microbiol. Infect. Dis.* **2013**, *75*, 115.
[42] H. Abbas, G. Shaker, R. Khattab, M. Askoura, *J. Microbiol., Biotechnol. Food Sci.* **2021**, 4232. https://doi.org/10.15414/jmbfs.4232.
[43] E. V. Capparelli, R. Bricker-Ford, M. J. Rogers, J. H. McKerrow, S. L. Reed, *Antimicrob. Agents Chemother.*, *61*, 01947.
[44] FDA, A.: Highlights of Prescribing Information, https://www.accessdata.fda.gov/drugsatfda_docs/label/2020/213036s000lbl.pdf (accessed: November 2021).
[45] D. R. Liston, M. Davis, *Clin. Cancer Res.* **2017**, *23*, 3489.
[46] M. D. Minden, D. E. Hogge, S. Weir, J. Kasper, L. Patton, Y. Jitkova, M. Gronda, R. Hurren, L. Rajewski, K. Schorno, H. Chang, J. M. Brandwein, V. Gupta, A. C. Schuh, S. Trudel, K. W. L. Yee, G. Reed, A. D. Schimmer, *Blood* **2012**, *120*, 1372.
[47] L. FDA, Highlights of Prescribing Information, https://www.accessdata.fda.gov/drugsatfda_docs/label/2018/020634s069lbl.pdf (accessed: November 2021).
[48] G. FDA, 500 mg (metformin hydrochloride extended release tablets) tablet https://www.accessdata.fda.gov/drugsatfda_docs/label/2006/021748s002lbl.pdf (accessed: November 2021).
[49] Antimicrobe, Mean Pharmacokinetics Parameters of Carbapenems in Healthy Volunteers at Steady State After Intravenous Infusions, http://www.antimicrobe.org/d12tab.htm#tab2 (accessed: November 2020).
[50] X. Liu, Y. Chen, H. Yang, J. Li, J. Yu, Z. Yu, G. Cao, X. Wu, Y. Wang, H. Wu, Y. Fan, J. Wang, J. Wu, Y. Jin, B. Guo, J. Hu, X. Bian, X. Li, J. Zhang, *Journal of Infection* **2021**, *82*, 207.
[51] https://www.accessdata.fda.gov/drugsatfda_docs/label/2008/050689s016lbl.pdf (accessed: November 2021).
[52] M. Nakashima, T. Uematsu, K. Kosuge, K. Umemura, H. Hakusui, M. Tanaka, *Antimicrob. Agents Chemother.* **1995**, *39*, 1015.
[53] FDA, https://www.accessdata.fda.gov/drugsatfda_docs/label/2019/200732s002lbl.pdf (accessed: November 2021).
[54] K. P. Davis, Y. Morales, A. L. McCabe, B. B. Aldridge, J. B. Mecsas, *bioRxiv* **2022**, 2022.
[55] K. Berthoin, C. S. Le Duff, J. Marchand-Brynaert, S. Carryn, P. M. Tulkens, *J. Antimicrob. Chemother.* **2010**, *65*, 1073.
[56] E. de Azambuja, J. F. Fleck, R. G. Batista, S. M. Barreto, *Pulm. Pharmacol. Ther.* **2005**, *18*, 363.
[57] https://www.cidrap.umn.edu/antimicrobial-stewardship/seattle-hospital-says-klebsiella-outbreak-has-infected-31-patients, **2023**.
[58] C. H. Chen, V. Gau, D. D. Zhang, J. C. Liao, F.-Y. Wang, P. K. Wong, *PLoS One* **2010**, *5*, e15472.
[59] E. Tekin, C. White, T. M. Kang, N. Singh, M. Cruz-Loya, R. Damoiseaux, V. M. Savage, P. J. Yeh, *NPJ Syst Biol Appl* **2018**, *4*, 31.
[60] K. Marimuthu, I. Venkatachalam, V. Koh, S. Harbarth, E. Perencevich, B. P. Z. Cherng, R. K. C. Fong, S. K. Pada, S. T. Ooi, N. Smitasin, K. C. Thoon, P. A. Tambyah, L. Y. Hsu, T. H. Koh, P. P. De, T. Y. Tan, D. Chan, R. N. Deepak, N. W. S. Tee, A. Kwa, Y. Cai, Y.-Y. Teo, N. M. Thevasagayam, S. R. S. Prakki, W. Xu, W. X. Khong, D. Henderson, N. Stoesser, D. W. Eyre, D. Crook, et al., *Nat. Commun.* **2022**, *13*, 3052.
[61] H. Xu, *Biometrika* **2005**, *92*, 385.
[62] H. Xu, J. Jaynes, X. Ding, *STAT SINICA* **2013**, https://doi.org/10.5705/ss.2012.210.